frontiers in Energy Research

BRIEF RESEARCH REPORT
published: 22 October 2021
doi: 10.3389/fenrg.2021.750600

Computationally Accelerated Discovery and Experimental Demonstration of $Gd_{0.5}La_{0.5}Co_{0.5}Fe_{0.5}O_3$ for Solar Thermochemical Hydrogen Production

OPEN ACCESS

Edited by:
Alicia Bayon,
Arizona State University, United States

Reviewed by:
Matteo Fasano,
Polytechnic University of Turin, Italy
Krishna Kamol Ghose,
University of New South Wales Canberra, Australia

***Correspondence:**
Eric N. Coker
encoker@sandia.gov

Specialty section:
This article was submitted to Solar Energy, a section of the journal Frontiers in Energy Research

Received: *30 July 2021*
Accepted: *05 October 2021*
Published: *22 October 2021*

Citation:
Park JE, Bare ZJL, Morelock RJ, Rodriguez MA, Ambrosini A, Musgrave CB, McDaniel AH and Coker EN (2021) Computationally Accelerated Discovery and Experimental Demonstration of $Gd_{0.5}La_{0.5}Co_{0.5}Fe_{0.5}O_3$ for Solar Thermochemical Hydrogen Production. Front. Energy Res. 9:750600. doi: 10.3389/fenrg.2021.750600

*James Eujin Park[1], Zachary J. L. Bare[2], Ryan J. Morelock[2], Mark A. Rodriguez[1], Andrea Ambrosini[1], Charles B. Musgrave[2,3,4], Anthony H. McDaniel[5] and Eric N. Coker[1]**

[1]Sandia National Laboratories, Albuquerque, NM, United States, [2]Department of Chemical and Biological Engineering, University of Colorado Boulder, Boulder, CO, United States, [3]Department of Chemistry, University of Colorado Boulder, Boulder, CO, United States, [4]Renewable and Sustainable Energy Institute, University of Colorado Boulder, Boulder, CO, United States, [5]Sandia National Laboratories, Livermore, CA, United States

Solar thermochemical hydrogen (STCH) production is a promising method to generate carbon neutral fuels by splitting water utilizing metal oxide materials and concentrated solar energy. The discovery of materials with enhanced water-splitting performance is critical for STCH to play a major role in the emerging renewable energy portfolio. While perovskite materials have been the focus of many recent efforts, materials screening can be time consuming due to the myriad chemical compositions possible. This can be greatly accelerated through computationally screening materials parameters including oxygen vacancy formation energy, phase stability, and electron effective mass. In this work, the perovskite $Gd_{0.5}La_{0.5}Co_{0.5}Fe_{0.5}O_3$ (GLCF), was computationally determined to be a potential water splitter, and its activity was experimentally demonstrated. During water splitting tests with a thermal reduction temperature of 1,350°C, hydrogen yields of 101 μmol/g and 141 μmol/g were obtained at re-oxidation temperatures of 850 and 1,000°C, respectively, with increasing production observed during subsequent cycles. This is a significant improvement from similar compounds studied before ($La_{0.6}Sr_{0.4}Co_{0.2}Fe_{0.8}O_3$ and $LaFe_{0.75}Co_{0.25}O_3$) that suffer from performance degradation with subsequent cycles. Confirmed with high temperature x-ray diffraction (HT-XRD) patterns under inert and oxidizing atmosphere, the GLCF mainly maintained its phase while some decomposition to $Gd_{2-x}La_xO_3$ was observed.

Keywords: concentrated solar energy, thermochemical water splitting, hydrogen, density functional theory, perovskite

INTRODUCTION

Solar thermochemical hydrogen (STCH) production has been studied as a potential path to produce alternative fuels (Miller et al., 2014). This reaction is generally a two-step process that generates hydrogen (H_2) gas by splitting water using metal oxide materials and concentrated solar energy (Steinfeld, 2005; Smestad and Steinfeld, 2012). In the first step of a typical STCH cycle, the metal oxide is thermally reduced under inert atmosphere at high temperature (>1,200°C, achieved using concentrated solar-thermal flux), creating oxygen vacancies in the metal oxide and releasing oxygen gas (Scheffe and Steinfeld, 2014). In the second re-oxidation step at a lower temperature under steam, the oxygen-deficient metal oxide splits water to produce H_2 gas while regenerating the metal oxide for consecutive water splitting cycles. While a combined photovoltaic/electrolytic system can be an alternative method for generating H_2 from water (Ivy, 2004), the efficiency of STCH systems were predicted to potentially exceed the efficiency of the combined system (Siegel et al., 2013).

Different classes of materials have been studied demonstrating STCH capabilities, including fluorites (CeO_2) (Gauckler et al., 1997; Abanades et al., 2010; Chueh et al., 2010; Scheffe and Steinfeld, 2014; Rao and Dey, 2017), iron oxides (Fe_3O_4) (Nakamura, 1977; Kodama et al., 2004; Coker et al., 2011; Scheffe and Steinfeld, 2014), and spinel ferrites (MFe_2O_4, M = Cu, Ni, Zn, etc.) (Tamaura et al., 1995; Allendorf et al., 2008; Miller et al., 2008; Fresno et al., 2009; Scheffe and Steinfeld, 2014). Additionally, perovskite oxides (ABO_3) have been investigated heavily with many perovskite materials demonstrated to possess water splitting capabilities (McDaniel et al., 2013; Yang et al., 2014; Rao and Dey, 2017; Barcellos et al., 2018; Nair and Abanades, 2018; Qian et al., 2020a; Qian et al., 2020b). A large chemical space of perovskite materials is available due to the flexibility in chemical compositions and crystal structures the formula can stabilize (Vasala and Karppinen, 2015). For this reason, perovskite oxides are fertile ground for discovering new STCH materials with high efficiencies.

With the vast composition space of inorganic materials, preliminary computational materials screening has become an important tool for accelerating materials discovery. Computational methods were previously applied to materials screening for the solid-state hydrogen storage reaction and chemical looping process (Clary et al., 2020; Singstock et al., 2020). For STCH, ternary (ABO_3) and quaternary ($AA'BO_3$) perovskites were explored to computationally evaluate their oxygen vacancy formation energies, electronic properties, and thermodynamic stabilities, with several promising candidate materials predicted based on these results (Emery et al., 2016; Sai Gautam et al., 2020). In this work, we report $Gd_{0.5}La_{0.5}Co_{0.5}Fe_{0.5}O_3$ (GLCF) as a new STCH material that was discovered using a computational screening approach and experimentally demonstrated as a STCH producing material.

METHODS

Computational Screening Framework

Potential STCH compounds from the $A_2BB'O_6$, $AA'B_2O_6$, and $AA'BB'O_6$ compositional spaces were first screened for stability as perovskites using the machine learned descriptor τ (Bartel et al., 2019). τ classifies potential perovskite compositions as perovskite or non-perovskite using the Shannon radii (rA, rB, rX) of the A, B, and X site ions and the formal oxidation state of the A site cation as inputs. This descriptor exhibits 92% accuracy for predicting theoretical perovskite synthesizability for ABX_3 compositions and 91% accuracy for $A_2BB'X_6$ compositions, where fractional weighting of the B site cation radii is used (Bartel et al., 2019). Of the compounds identified by τ as synthesizable as perovskites, the STCH relevant properties of >1,000 Gd-containing compositions were evaluated in a high-throughput optimization scheme (Bare et al., 2021a). The compositions La_2CoFeO_6, $GdLaCoFeO_6$, and Gd_2CoFeO_6 are predicted by τ to be stable as perovskites (with formal oxidation states of +3 used for Gd, La, Co, and Fe and -2 used for O) and are predicted by DFT to have favorable STCH properties (see Results and Discussion).

PySPuDS (Bare et al., 2021b), a custom high-throughput python wrapper for the bond valence method (BVM) based Structure Prediction and Diagnostic Software (SPuDS), was used to generate initial perovskite geometries for DFT optimization (Lufaso and Woodward, 2001). The BVM Global Instability Index (GII), which SPuDS minimizes to predict the phase and magnitude of perovskite octahedral tilting, is strongly correlated with DFT energy in perovskite oxides (Morelock et al., 2021). This enables SPuDS to accurately predict perovskite ground state polymorph structures consistent with DFT, thereby substantially reducing the computational expense associated with high-throughput DFT investigations (Bare et al., 2021b). Initial geometries for DFT optimizations of the La_2CoFeO_6, $GdLaCoFeO_6$, and Gd_2CoFeO_6 perovskites were generated in the a-b+a- Glazer mode, as this is the ground state tilting mode most frequently predicted by DFT for experimentally observed ABO_3 perovskite oxides (Bare et al., 2021b). Atomic configurations for cation alloying on the B site were generated using rock salt site ordering, while configurations for alloying on the A sites were generated that minimize the Ewald sum.

The specific pseudopotentials and Hubbard +U parameters used for GGA+U DFT optimizations are compatible with the Materials Project (MP) database (Jain et al., 2013), which tabulates the structures and energies of >130,000 inorganic materials. Calculations were performed using the Vienna Ab initio Simulation Program (VASP 5.4.1) (Kresse and Hafner, 1993; Kresse and Hafner, 1994; Kresse and Furthmüller, 1996a; Kresse and Furthmüller, 1996b) with periodic boundary conditions utilizing projector augmented wave (PAW) pseudopotentials (Kresse and Joubert, 1999) and the Perdew-Burke-Ernzerhof (PBE) exchange-correlation functional (Perdew et al., 1996). +U parameters of 3.32 and 5.3 were used for Co^{3+} and Fe^{3+}, respectively, consistent with pymatgen's MPRelaxSet (Jain et al., 2013). The electronic wave functions were expanded in a plane wave basis with an energy cutoff of 520 eV. The Brillouin

zones were sampled during geometry optimizations using an automatically generated Γ-centered Monkhorst-Pack k-point mesh with a grid density of at least 1,000/(atoms/unit cell). Oxide-specific corrections to DFT total energies were included to maintain compatibility with the MP (Jain et al., 2013).

We explicitly considered the effects of magnetism by first performing two consecutive spin-polarized relaxations initialized in a high-spin ferromagnetic configuration with species-specific initial magnetic moments dictated by the default MP spin parameters. Then, magnetic sampling of the computed structures was performed for up to 20 different magnetic symmetries using pymatgen's MagneticStructureEnumerator (Ong et al., 2013). Finally, the internal coordinates of the DFT structures–with lattice vectors and initial magnetic moments fixed from previous optimizations–were optimized such that total energies were converged to within 10^{-6} eV, and forces converged to within 0.01 eV/Å. The effects of spin configuration on the electronic density of states (DOS) were also explicitly described in this manner. Calculations to determine oxygen vacancy energies were performed using the aforementioned convergence criteria for all symmetrically unique vacancies at a defect concentration of $C_d = 0.0833$.

Materials

All chemicals and gases were purchased and used as-received: gadolinium (III) oxide (Gd_2O_3, Alfa Aesar, 99.999%), lanthanum (III) oxide (La_2O_3, Aldrich, 99.99%), cobalt (II, III) oxide (Co_3O_4, Alfa Aesar, 99.99%), and iron (III) oxide (Fe_2O_3, Acros Organics, 99.999%), argon gas (Matheson, UHP grade), and air (Matheson, ultra-zero grade).

Synthesis of $Gd_{0.5}La_{0.5}Co_{0.5}Fe_{0.5}O_3$

Synthesis was conducted via a solid state synthesis route. For a 2 g scale reaction, stoichiometric amounts of gadolinium (III) oxide (0.7151 g), lanthanum (III) oxide (0.6427 g), cobalt (II, III) oxide (0.3167 g), and iron (III) oxide (0.3150 g) were ground by hand in an agate mortar and pestle for ~10 min. The resulting powder mixture was calcined in air at 600°C (5°C/min, 12 h dwell), then sintered in air at 1,300°C (9°C/min, 12 h dwell) with intermediate grinding.

Characterization

Powder X-ray diffraction (XRD) was collected on Bruker D2 Phaser X-ray Diffractometer with Cu Kα radiation. Profile fitting of diffraction patterns were performed with GSAS-II (Toby and Von Dreele, 2013). Thermogravimetric analysis (TGA) was performed on a Netzsch STA 449 F1 Jupiter thermal analyzer.

Thermochemical cycling experiments were conducted under gas flow rates of 100 ml/min. For thermal reduction under Ar (100 ml/min), the sample (~50 mg) was first heated to 1,250°C (10°C/min), held isothermally for 30 min (thermal reduction), cooled to 400°C (25°C/min), then held isothermally for 30 min. For re-oxidation, the gas was switched to a mixture of air (80 ml/min) and Ar (20 ml/min), and the sample was heated to 1,100°C (10°C/min), isothermally held for 30 min, then cooled to 200°C (25°C/min). For repeated consecutive analyses, the sample was re-weighed between runs. TGA baseline correction was performed with an empty crucible. All thermograms shown here are corrected.

Water splitting experiments were conducted in a stagnation flow reactor (SFR) equipped with a laser-based sample heater and a mass spectrometer; the experimental details are described in previous papers (Scheffe et al., 2011; Arifin et al., 2012; Scheffe et al., 2013). In brief, the powder sample was placed in a tube furnace to maintain the oxidation temperature, and then irradiated by an IR laser through an optical access window to achieve the desired reduction temperature. The amount of oxygen gas evolved during reduction under Ar and hydrogen gas evolved during oxidation under 40 vol% steam were measured using a mass spectrometer.

High temperature XRD (HT-XRD) was performed on a Scintag PAD X-ray diffractometer, equipped with a Buehler hot-stage with Pt/Rh heating strip and surround heater. The hot stage resides within a sealed chamber with an X-ray-transparent beryllium window, and gas flow (either helium or air) was maintained at 200 ml/min. The data was analyzed using MDI Jade 8.2 software, and the plot was constructed with square root of intensity to easily observe low intensity peaks.

RESULTS AND DISCUSSION

To evaluate compound stability relative to decomposition, the DFT computed energies of the La_2CoFeO_6 (L2CF), $GdLaCoFeO_6$ (GLCF), and Gd_2CoFeO_6 (G2CF) perovskites optimized in the monoclinic, triclinic, and monoclinic space groups, respectively, (**Supplementary Figure S1**) were compared to the DFT computed energies of their potential decomposition products tabulated in the MP database. The energy of a material relative to the convex hull, E_{hull}, quantifies a material's stability relative to its decomposition products. Monoclinic L2CF, triclinic GLCF, and monoclinic G2CF exhibit E_{hull} of 0, 6.8, and 0 meV/atom, respectively, predicting that all three STCH candidates can be successfully synthesized as perovskites relative to their competing phases. The combination of the τ-predicted stabilities and E_{hull} values of L2CF, GLCF, and G2CF suggests that Gd-La-Co-Fe-O is a promising compositional space for experimentally synthesizable perovskite oxides. We thus selected L2CF, GLCF, and G2CF from our high-throughput screening and computed additional STCH-relevant properties for these compounds, including DOS and charge neutral oxygen vacancy formation enthalpies (ΔH_{Ovac}).

The distributions of ΔH_{Ovac} computed by DFT for the symmetrically unique sites of L2CF, GLCF, and G2CF are shown in **Figure 1A**. The ΔH_{Ovac} distribution of GLCF is bounded by the ΔH_{Ovac} distributions of L2CF (lower bound) and G2CF (upper bound). Herein, we use the DFT computed ΔH_{Ovac} of CeO_2 (3.95 eV/atom) (Abanades and Flamant, 2006; Chueh and Haile, 2010), the gold standard STCH redox mediator (Muhich et al., 2016), as the upper bound for the STCH active range and a liberal lower bound of 2 eV/atom to account for uncertainty in DFT energetics (Naghavi et al., 2020). Materials approaching the minimum ΔH_{Ovac} for STCH activity exhibit slow oxidation kinetics and/or degradation during redox cycling,

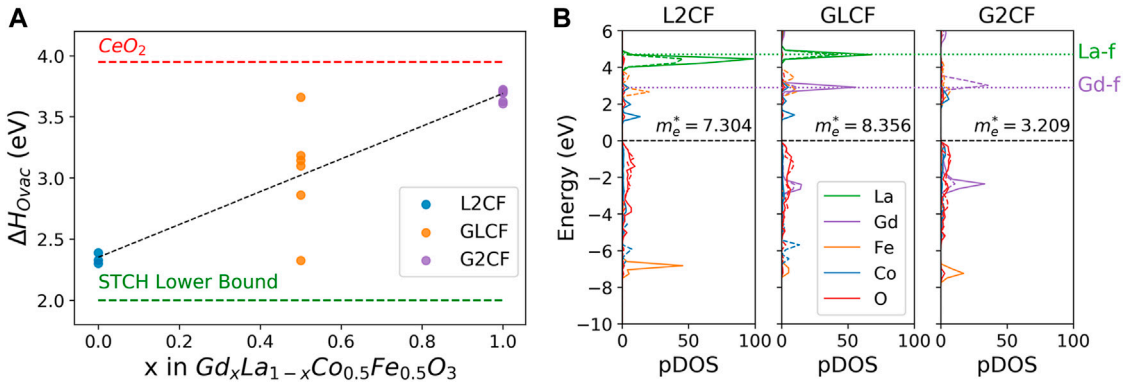

FIGURE 1 | (A) Computed ΔH_{Ovac} values vs Gd concentration (x) in $Gd_xLa_{1-x}Co_{0.5}Fe_{0.5}O_3$, showing that higher x increases ΔH_{Ovac}, thus the stability of oxygen. All three materials studied are within the estimated STCH active range (2.0 eV ≤ ΔH_{Ovac} ≤ 3.95 eV). The mean vacancy enthalpy ΔH_{Ovac} is described by the equation, ΔH_{Ovac} = 1.34x + 2.35 (R^2 = 0.999), where x is the fractional concentration of Gd on the A site. **(B)** DFT computed DOS for La_2CoFeO_6 (L2CF), $GdLaCoFeO_6$ (GLCF), and Gd_2CoFeO_6 (G2CF). For GLCF, a larger multiplicity of Gd-f orbitals closer to the conduction band minimum than La-f orbitals is shown, leading to the largest calculated DOS electron effective mass at 1000 K (m_e = 8.356).

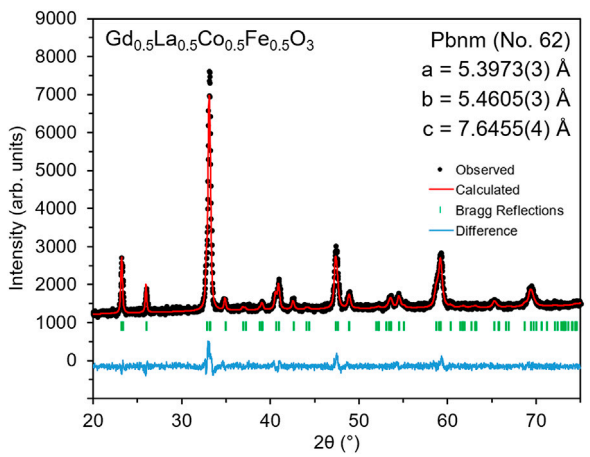

FIGURE 2 | Room temperature XRD pattern with LeBail profile fitting for $Gd_{0.5}La_{0.5}Co_{0.5}Fe_{0.5}O_3$, showing it to be isostructural to the orthorhombic perovskite, $LaFeO_3$ (Proskurnina et al., 2007).

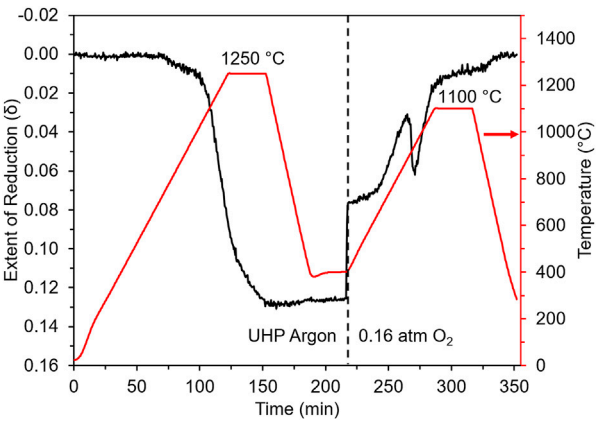

FIGURE 3 | TGA results of the second redox cycle showing redox behavior of GLCF. The red curve corresponds to the sample temperature, and the black line corresponds to the extent of reduction (δ in $Gd_{0.5}La_{0.5}Co_{0.5}Fe_{0.5}O_{3-\delta}$).

whereas materials approaching the maximum ΔH_{Ovac} for STCH activity suffer from reduced H_2 capacity (Muhich et al., 2016). GLCF exhibits both O vacancies with low and high ΔH_{Ovac}, where vacancies with low ΔH_{Ovac} participate in H_2 production and those with high ΔH_{Ovac} are less likely to form under STCH operating conditions and therefore enable preservation of the perovskite lattice during redox cycling. This ΔH_{Ovac} distribution predicts enhanced cyclability of GLCF relative to L2CF and increased H_2 production capacity relative to G2CF.

Additionally, GLCF exhibits a large DOS effective mass, m_e, that arises from its large concentration of accessible electronic states near the conduction band minimum (CBM). Lany showed that large m_e corresponds with large electronic contributions to the entropy of reduction S_{red} in STCH processes (Lany, 2018) that benefits STCH performance at high temperatures (Meredig and Wolverton, 2009). **Figure 1B** shows the DFT computed DOS for L2CF, GLCF, and G2CF. GLCF exhibits a larger DOS m_e at 1000 K (m_e = 8.356) than both L2CF (m_e = 7.304) and G2CF (m_e = 3.209). The introduction of Gd into the nominally La-occupied A site of L2CF results in unoccupied states that lie closer to the CBM than those of La alone, which increases m_e. However, complete substitution of Gd for La increases the splitting of the unoccupied Gd-f states that results in lowering m_e relative to GLCF. Due to its favorable ΔH_{Ovac} distribution and larger m_e relative to L2CF and G2CF, GLCF was recommended for experimental synthesis and characterization of STCH performance.

The room temperature XRD pattern of the synthesized GLCF is shown in **Figure 2**. The resulting material is isostructural to $LaFeO_3$, $GdFeO_3$, and $La_{1-x}Gd_xFeO_3$ (x = 0, 0.2, 0.5, 0.8, and 1), which are all orthorhombic perovskites (Proskurnina et al., 2007; Wiglusz et al., 2015; Orlov et al., 2016). LeBail profile fitting analysis was performed, confirming the GLCF crystalizes in the Pbnm space group (No. 62) with no additional secondary phases. The lattice parameters for GLCF (a = 5.3973(3) Å, b = 5.4605(3)

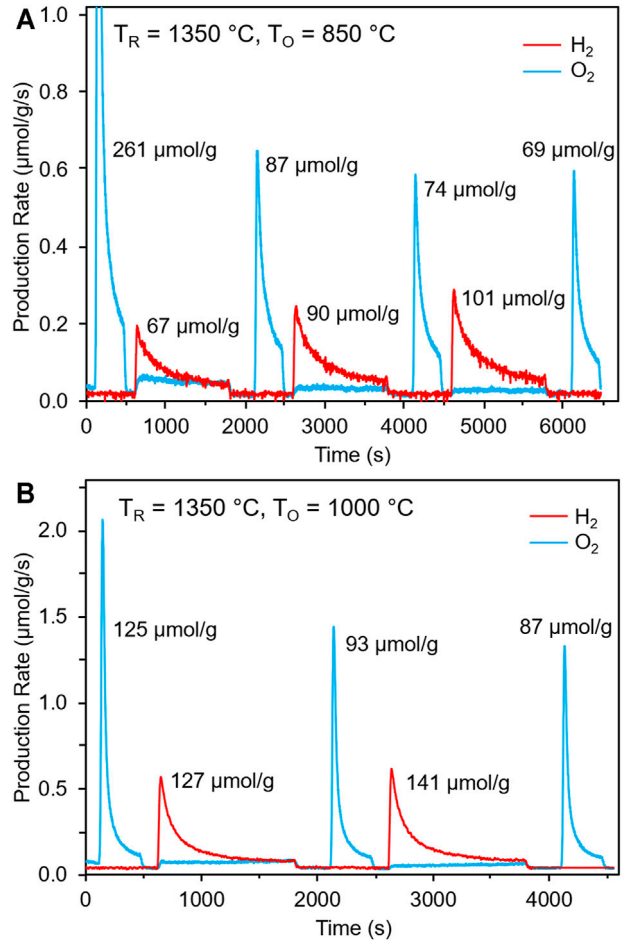

FIGURE 4 | Water splitting experiment on GLCF at T_R = 1,350°C (330 s) and **(A)** T_O = 850°C and **(B)** T_O = 1,000°C with 40 vol% H_2O (1,200 s).

Å, c = 7.6455(4) Å) are slightly smaller than $LaFeO_3$ (a = 5.5506(6) Å, b = 5.5608(5) Å, c = 7.8464(9) Å) (Proskurnina et al., 2007). This is likely due to the smaller atomic radii of Gd and Co compared to La and Fe, respectively (Shannon, 1976).

The redox behavior of GLCF was examined through thermogravimetric analysis (TGA), which monitors the mass change with respect to temperature and atmosphere (Ar or air). In the case of these materials, the mass change corresponds to gain/loss of oxygen. The mass change was converted to the extent of reduction (δ), assuming $Gd_{0.5}La_{0.5}Co_{0.5}Fe_{0.5}O_{3-\delta}$ during redox cycling. The as-prepared powder was subjected to redox cycles, comprising a reduction step at 1,250°C under Ar followed by a re-oxidation step at 1,100°C under air, corresponding to 0.16 atm O_2. The redox cycle was repeated twice with the two redox cycles showing similar behavior. The second redox cycle is shown in **Figure 3**. During thermal reduction, a shallow weight loss was observed at ~750°C, followed by a steeper weight loss onset at ~1,030°C. After the isotherm at 1,250°C, the extent of reduction (δ) was ~0.13. During re-oxidation, the mass sharply increased when the gas was switched from Ar to air at 400°C, followed by a more gradual increase as the temperature was raised. The dip in the extent of reduction seen between 900 and 1,100°C is attributed to a phase change in the material, that is, formation of a phase at around 900°C that ejects oxygen to achieve stability. This change in δ is reproducible between cycles. The sample mass returns to the starting mass after the re-oxidation step.

The water splitting capability of GLCF was verified using a stagnation flow reactor (SFR). **Figure 4** shows the water splitting results performed with a thermal reduction temperature (T_R) of 1,350°C for 330 s and re-oxidation temperatures (T_O) of 850 and 1,000°C for 1,200 s under 40 vol% H_2O. Water splitting was observed under both sets of conditions, with the amount of H_2 produced increasing with each cycle. For T_O = 850°C (**Figure 4A**), the amount of H_2 produced was 67, 90, and 101 μmol/g for each consecutive cycle. Moreover, significantly less O_2 was released in the second reduction cycle compared to the first cycle, likely due to the water splitting step being kinetically limited. This is also evident from the long tails of H_2 gas evolved during the re-oxidation steps. For T_O = 1,000°C (**Figure 4B**), the H_2 capacity increased (127 and 141 μmol/g), evident of an improvement in the rate of water splitting at higher temperature. Similar to the T_O = 850°C experiment, more H_2 was produced as cycle-number increased. In an ideal situation, once steady state has been achieved, the amount of H_2 should be twice of the amount of O_2 produced. From the SFR experiments with repeated cycles, GLCF is evolving and approaching this ideal steady state, though additional studies are needed to understand this behavior.

While $LaFeO_3$ was previously reported to have negligible solar thermochemical H_2O and CO_2 conversion behavior (Jiang et al., 2014; Chen et al., 2017), similar perovskites to GLCF, $La_{0.6}Sr_{0.4}Co_{0.2}Fe_{0.8}O_3$ and $LaFe_{0.75}Co_{0.25}O_3$, were shown to be active for solar thermochemical CO_2 conversion (STCH activity is unknown) (Nair and Abanades, 2018), indicating that the mixing of Co and Fe may have contributed to the solar thermochemical conversion activity. For $La_{0.6}Sr_{0.4}Co_{0.2}Fe_{0.8}O_3$ and $LaFe_{0.75}Co_{0.25}O_3$, however, CO production decreased substantially during subsequent cycles (Nair and Abanades, 2018). The substitution of Gd for La may have contributed to minimizing performance degradation as predicted by DFT calculations.

In terms of its water splitting ability, at T_R = 1,350°C and T_O = 850°C, GLCF produced more H_2 (101 μmol/g) than CeO_2 (50 μmol/g) (Barcellos et al., 2018). However, GLCF produced less H_2 compared to the previously studied perovskite materials $BaCe_{0.25}Mn_{0.75}O_3$ (BCM) and $Sr_{0.4}La_{0.6}Mn_{0.6}Al_{0.4}O_3$ (SLMA4664) (McDaniel et al., 2013; Barcellos et al., 2018). BCM and SLMA4664 produced 140 μmol/g (T_R = 1,350°C, T_O = 850°C) and 307 μmol/g (T_R = 1,350°C, T_O = 1,000°C) of H_2, respectively (McDaniel et al., 2013; Barcellos et al., 2018). However, direct comparisons of performance reported for different conditions (temperature, atmosphere, and time) for various materials that have different optimized conditions for STCH can lead to incorrect conclusions about the H_2 production capabilities of candidate materials. In the present case, the water splitting experimental conditions implemented for GLCF have not yet been optimized. Nevertheless, computational screening

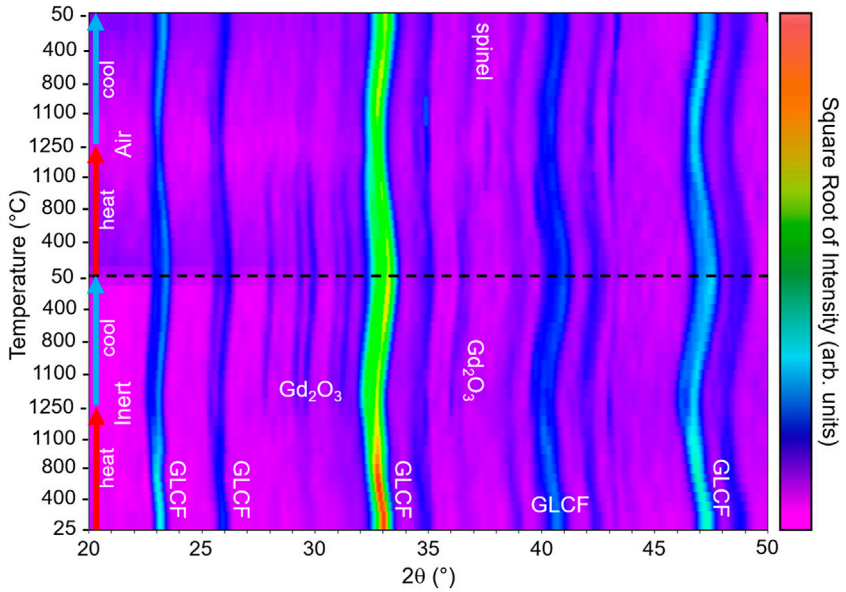

FIGURE 5 | HT-XRD pattern of GLCF, heating from room temperature to 1,250°C then cooling to 50°C under He flow, followed by the identical thermal profile under air. The experiment progresses from the bottom of the plot to the top.

greatly accelerated the discovery of GLCF as a water splitting material, which would otherwise have been experimentally time consuming due to the vast chemical space of perovskite materials.

To understand the phase stability in GLCF during redox cycling, HT-XRD patterns were collected first from room temperature to 1,250°C to 50°C under He for thermal reduction, then with an identical temperature profile under air for re-oxidation. The GLCF sample was redox-cycled (T_R = 1,250°C under Ar, T_O = 1,100°C under air) before collecting the HT-XRD patterns. The HT-XRD pattens are shown in **Figure 5**. During the HT-XRD experiment, GLCF appears to maintain its perovskite phase as the major phase, but the major peaks broaden and exhibit some peak splitting occurring during reduction. In addition to the changes in the major GLCF phase, during cool down at ~1,200°C under He, additional peaks appear corresponding to Gd_2O_3 phase. Due to the shift in peaks, it may have different chemistry (i.e. $Gd_{2-x}La_xO_3$). The additional Gd_2O_3 phase remains in the pattern until heated under air at ~700–800°C during re-oxidation. The disappearance of the Gd_2O_3 phase may correspond to the increase in the extent of reduction observed in the TG experiment at ~900°C during reoxidation. Moreover, a spinel phase appears during cool down under air. Overall, during the redox cycle, the perovskite phase persists, agreeing with the stable STCH activity observed in the SFR results and TGA cycling tests.

CONCLUSION

Solar thermochemical hydrogen production (STCH) significantly contributes to the renewable energy portfolio. However, materials discovery with high efficiency is needed, and computational screening can greatly accelerate this process. This was demonstrated with $Gd_{0.5}La_{0.5}Co_{0.5}Fe_{0.5}O_3$ (GLCF), a perovskite oxide, that was computationally determined first, then experimentally demonstrated. When compared to $LaCo_{0.5}Fe_{0.5}O_3$, it was predicted that GLCF would have higher phase stability due to the incorporation of Gd on the La site. The synthesis of a single phase GLCF sample was achieved. With redox activity confirmed through thermogravimetric analysis, stable water splitting behavior over multiple cycles was also observed. When compared to previously reported $La_{0.6}Sr_{0.4}Co_{0.2}Fe_{0.8}O_3$ and $LaFe_{0.75}Co_{0.25}O_3$, which suffered from performance degradation with subsequent cycles, the Gd substitution of La plays a significant role to maintain water splitting performance. Based on high temperature x-ray diffraction experiments, the GLCF perovskite phase persists which potentially contributes to the stable water splitting performance. This work demonstrates that computational materials screening can greatly accelerate the discovery of new water splitting materials. Through computational screening, potential water splitting materials were narrowed down to a promising STCH material from the vast chemical space of perovskite materials, and a unique strategy of incorporating a rare earth element that improved the stability was demonstrated.

DATA AVAILABILITY STATEMENT

The original contributions presented in the study are included in the article/**Supplementary Material**, further inquiries can be directed to the corresponding author.

AUTHOR CONTRIBUTIONS

JP conducted material synthesis and characterization and drafted the manuscript. ZB and RM conducted the DFT calculations and wrote sections of the manuscript. MR, AM, and EC conducted materials characterization. AA provided guidance on material synthesis. CM supervised the DFT calculations.

FUNDING

This work was supported by the U.S. Department of Energy (DOE), Office of Energy Efficiency and Renewable Energy (EERE), Hydrogen and Fuel Cell Technologies Office (HFTO), and specifically the HydroGEN Advanced Water Splitting Materials Consortium, established as part of the Energy Materials Network under this same office (award DE-EE0008088). CM, ZB and RM also acknowledge support from the National Science Foundation, awards NSF CHEM-1800592 and CBET-2016225. Sandia National Laboratories is a multi-mission laboratory managed and operated by National Technology and Engineering Solutions of Sandia, LLC., a wholly owned subsidiary of Honeywell International, Inc., for the U.S. Department of Energy's National Nuclear Security Administration under contract DE-NA0003525. The views expressed in this article do not necessarily represent the views of the U.S. Department of Energy or the United States Government.

SUPPLEMENTARY MATERIAL

The Supplementary Material for this article can be found online at: https://www.frontiersin.org/articles/10.3389/fenrg.2021.750600/full#supplementary-material

REFERENCES

Abanades, S., and Flamant, G. (2006). Thermochemical Hydrogen Production from a Two-step Solar-Driven Water-Splitting Cycle Based on Cerium Oxides. *Solar Energy* 80 (12), 1611–1623. doi:10.1016/j.solener.2005.12.005

Abanades, S., Legal, A., Cordier, A., Peraudeau, G., Flamant, G., and Julbe, A. (2010). Investigation of Reactive Cerium-Based Oxides for H2 Production by Thermochemical Two-step Water-Splitting. *J. Mater. Sci.* 45 (15), 4163–4173. doi:10.1007/s10853-010-4506-4

Allendorf, M. D., Diver, R. B., Siegel, N. P., and Miller, J. E. (2008). Two-Step Water Splitting Using Mixed-Metal Ferrites: Thermodynamic Analysis and Characterization of Synthesized Materials. *Energy Fuels* 22 (6), 4115–4124. doi:10.1021/ef8005004

Arifin, D., Aston, V. J., Liang, X., McDaniel, A. H., and Weimer, A. W. (2012). CoFe2O4 on a Porous Al2O3 Nanostructure for Solar Thermochemical CO2 Splitting. *Energy Environ. Sci.* 5 (11), 9438–9443. doi:10.1039/C2EE22090C

Bartel, C. J., Sutton, C., Goldsmith, B. R., Ouyang, R., Musgrave, C. B., Ghiringhelli, L. M., et al. (2019). New Tolerance Factor to Predict the Stability of Perovskite Oxides and Halides. *Sci. Adv.* 5 (2), eaav0693. doi:10.1126/sciadv.aav0693

Chen, Z., Jiang, Q., Tong, J., Yang, M., Jiang, Z., and Li, C. (2017). Enhancement Effects of Dopants and SiO2 Support on Mixed Metal Ferrites Based Two-step Thermochemical Water Splitting. *Solar Energy* 144, 643–659. doi:10.1016/j.solener.2017.01.049

Chueh, W. C., Falter, C., Abbott, M., Scipio, D., Furler, P., Haile, S. M., et al. (2010). High-Flux Solar-Driven Thermochemical Dissociation of CO2 and H2O Using Nonstoichiometric Ceria. *Science* 330 (6012), 1797–1801. doi:10.1126/science.1197834

Chueh, W. C., and Haile, S. M. (2010). A Thermochemical Study of Ceria: Exploiting an Old Material for New Modes of Energy Conversion and CO 2 Mitigation. *Phil. Trans. R. Soc. A.* 368 (1923), 3269–3294. doi:10.1098/rsta.2010.0114

Clary, J. M., Holder, A. M., and Musgrave, C. B. (2020). Computationally Predicted High-Throughput Free-Energy Phase Diagrams for the Discovery of Solid-State Hydrogen Storage Reactions. *ACS Appl. Mater. Inter.* 12 (43), 48553–48564. doi:10.1021/acsami.0c13298

Coker, E. N., Ambrosini, A., Ambrosini, A., Rodriguez, M. A., and Miller, J. E. (2011). Ferrite-YSZ Composites for Solar Thermochemical Production of Synthetic Fuels: in Operando Characterization of CO2 Reduction. *J. Mater. Chem.* 21 (29), 10767–10776. doi:10.1039/C1JM11053E

Emery, A. A., Saal, J. E., Kirklin, S., Hegde, V. I., and Wolverton, C. (2016). High-Throughput Computational Screening of Perovskites for Thermochemical Water Splitting Applications. *Chem. Mater.* 28 (16), 5621–5634. doi:10.1021/acs.chemmater.6b01182

Fresno, F., Fernández-Saavedra, R., Belén Gómez-Mancebo, M., Vidal, A., Sánchez, M., Isabel Rucandio, M., et al. (2009). Solar Hydrogen Production by Two-step Thermochemical Cycles: Evaluation of the Activity of Commercial Ferrites. *Int. J. Hydrogen Energ.* 34 (7), 2918–2924. doi:10.1016/j.ijhydene.2009.02.020

Gauckler, L. J., Go¨dickemeier, M., and Schneider, D. (1997). Nonstoichiometry and Defect Chemistry of Ceria Solid Solutions. *J. Electroceram.* 1 (2), 165–172. doi:10.1023/A:1009928817542

Ivy, J. (2004). "Summary of Electrolytic Hydrogen Production," NREL/MP-560-36734, Colorado: National Renewable Energy Laboratory.

Jain, A., Ong, S. P., Hautier, G., Chen, W., Richards, W. D., Dacek, S., et al. (2013). Commentary: The Materials Project: A Materials Genome Approach to Accelerating Materials Innovation. *APL Mater.* 1 (1), 011002. doi:10.1063/1.4812323

Jiang, Q., Tong, J., Zhou, G., Jiang, Z., Li, Z., and Li, C. (2014). Thermochemical CO2 Splitting Reaction with Supported LaxA1−xFeyB1−yO3 (A=Sr, Ce, B=Co, Mn; 0⩽x, Y⩽1) Perovskite Oxides. *Solar Energy* 103, 425–437. doi:10.1016/j.solener.2014.02.033

Kodama, T., Nakamuro, Y., and Mizuno, T. (2004). A Two-step Thermochemical Water Splitting by Iron-Oxide on Stabilized Zirconia. *J. Sol. Energ. Eng.* 128 (1), 3–7. doi:10.1115/1.1878852

Kresse, G., and Furthmüller, J. (1996a). Efficiency of Ab-Initio Total Energy Calculations for Metals and Semiconductors Using a Plane-Wave Basis Set. *Comput. Mater. Sci.* 6 (1), 15–50. doi:10.1016/0927-0256(96)00008-0

Kresse, G., and Furthmüller, J. (1996b). Efficient Iterative Schemes Forab Initiottotal-Energy Calculations Using a Plane-Wave Basis Set. *Phys. Rev. B* 54 (16), 11169–11186. doi:10.1103/PhysRevB.54.11169

Kresse, G., and Hafner, J. (1993). Ab Initiomolecular Dynamics for Liquid Metals. *Phys. Rev. B* 47 (1), 558–561. doi:10.1103/PhysRevB.47.558

Kresse, G., and Hafner, J. (1994). Ab Initiomolecular-Dynamics Simulation of the Liquid-Metal-Amorphous-Semiconductor Transition in Germanium. *Phys. Rev. B* 49 (20), 14251–14269. doi:10.1103/PhysRevB.49.14251

Kresse, G., and Joubert, D. (1999). From Ultrasoft Pseudopotentials to the Projector Augmented-Wave Method. *Phys. Rev. B* 59 (3), 1758–1775. doi:10.1103/PhysRevB.59.1758

Lany, S. (2018). Communication: The Electronic Entropy of Charged Defect Formation and its Impact on Thermochemical Redox Cycles. *J. Chem. Phys.* 148 (7), 071101. doi:10.1063/1.5022176

Lufaso, M. W., and Woodward, P. M. (2001). Prediction of the Crystal Structures of Perovskites Using the Software Program SPuDS. *Acta Crystallogr. Sect B* 57, 725–738. doi:10.1107/s0108768101015282

McDaniel, A. H., Miller, E. C., Arifin, D., Ambrosini, A., Coker, E. N., O'Hayre, R., et al. (2013). Sr- and Mn-Doped LaAlO3−δ for Solar Thermochemical H2 and CO Production. *Energ. Environ. Sci.* 6 (8), 2424–2428. doi:10.1039/C3EE41372A

Meredig, B., and Wolverton, C. (2009). First-principles Thermodynamic Framework for the Evaluation of thermochemicalH2O- orCO2-Splitting Materials. *Phys. Rev. B* 80 (24), 245119. doi:10.1103/PhysRevB.80.245119

Miller, J. E., Allendorf, M. D., Diver, R. B., Evans, L. R., Siegel, N. P., and Stuecker, J. N. (2008). Metal Oxide Composites and Structures for Ultra-high

Temperature Solar Thermochemical Cycles. *J. Mater. Sci.* 43 (14), 4714–4728. doi:10.1007/s10853-007-2354-7

Miller, J. E., McDaniel, A. H., and Allendorf, M. D. (2014). Considerations in the Design of Materials for Solar-Driven Fuel Production Using Metal-Oxide Thermochemical Cycles. *Adv. Energ. Mater.* 4 (2), 1300469. doi:10.1002/aenm.201300469

Morelock, R., Bare, Z. J. L., and Musgrave, C. B. (2021). Bond Valence Parameterization for the Accurate Description of DFT Energetics in ABO3 Perovskites. *under Rev.*

Muhich, C. L., Ehrhart, B. D., Al-Shankiti, I., Ward, B. J., Musgrave, C. B., and Weimer, A. W. (2016). A Review and Perspective of Efficient Hydrogen Generation via Solar Thermal Water Splitting. *Wires Energ. Environ* 5 (3), 261–287. doi:10.1002/wene.174

Naghavi, S. S., He, J., and Wolverton, C. (2020). CeTi2O6-A Promising Oxide for Solar Thermochemical Hydrogen Production. *ACS Appl. Mater. Inter.* 12 (19), 21521–21527. doi:10.1021/acsami.0c01083

Nair, M. M., and Abanades, S. (2018). Experimental Screening of Perovskite Oxides as Efficient Redox Materials for Solar Thermochemical CO2 Conversion. *Sustainable Energ. Fuels* 2 (4), 843–854. doi:10.1039/C7SE00516D

Nakamura, T. (1977). Hydrogen Production from Water Utilizing Solar Heat at High Temperatures. *Solar Energy* 19 (5), 467–475. doi:10.1016/0038-092X(77)90102-5

Ong, S. P., Richards, W. D., Jain, A., Hautier, G., Kocher, M., Cholia, S., et al. (2013). Python Materials Genomics (Pymatgen): A Robust, Open-Source Python Library for Materials Analysis. *Comput. Mater. Sci.* 68, 314–319. doi:10.1016/j.commatsci.2012.10.028

Orlov, Y. S., Dudnikov, V. A., Gorev, M. V., Vereshchagin, S. N., Solov'ev, L. A., and Ovchinnikov, S. G. (2016). Thermal Properties of Rare Earth Cobalt Oxides and of La1-X Gd X CoO3 Solid Solutions. *Jetp Lett.* 103 (9), 607–612. doi:10.1134/S0021364016090058

Perdew, J. P., Burke, K., and Ernzerhof, M. (1996). Generalized Gradient Approximation Made Simple. *Phys. Rev. Lett.* 77 (18), 3865–3868. doi:10.1103/PhysRevLett.77.3865

Proskurnina, N. V., Voronin, V. I., Cherepanov, V. A., and Kiselev, E. A. (2007). Phase Equilibria and crystal Structure of the Solid Solution LaFe1−xNixO3−δ (0≤x≤1). *Prog. Solid State. Chem.* 35 (2), 233–239. doi:10.1016/j.progsolidstchem.2007.01.022

Qian, X., He, J., Mastronardo, E., Baldassarri, B., Wolverton, C., and Haile, S. M. (2020a). Favorable Redox Thermodynamics of SrTi0.5Mn0.5O3−δ in Solar Thermochemical Water Splitting. *Chem. Mater.* 32, 9335–9346. doi:10.1021/acs.chemmater.0c03278

Qian, X., He, J., Mastronardo, E., Baldassarri, B., Yuan, W., Wolverton, C., et al. (2021b). Outstanding Properties and Performance of CaTi0.5Mn0.5O3-δ for Solar-Driven Thermochemical Hydrogen Production. *Matter* 4, 688–708. doi:10.1016/j.matt.2020.11.016

Rao, C. N. R., and Dey, S. (2017). Solar Thermochemical Splitting of Water to Generate Hydrogen. *Proc. Natl. Acad. Sci. U S A.* 114 (51), 13385–13393. doi:10.1073/pnas.1700104114

R. Barcellos, D., Sanders, M. D., Tong, J., McDanielA.Hand O'Hayre, R. P. (2018). BaCe0.25Mn0.75O3−δ-a Promising Perovskite-type Oxide for Solar Thermochemical Hydrogen Production. *Energ. Environ. Sci.* 11 (11), 3256–3265. doi:10.1039/C8EE01989D

Sai Gautam, G., Stechel, E. B., and Carter, E. A. (2020). Exploring Ca-Ce-M-O (M = 3d Transition Metal) Oxide Perovskites for Solar Thermochemical Applications. *Chem. Mater.* 32 (23), 9964–9982. doi:10.1021/acs.chemmater.0c02912

Scheffe, J. R., Allendorf, M. D., Coker, E. N., Jacobs, B. W., McDaniel, A. H., and Weimer, A. W. (2011). Hydrogen Production via Chemical Looping Redox Cycles Using Atomic Layer Deposition-Synthesized Iron Oxide and Cobalt Ferrites. *Chem. Mater.* 23 (8), 2030–2038. doi:10.1021/cm103622e

Scheffe, J. R., McDaniel, A. H., Allendorf, M. D., and Weimer, A. W. (2013). Kinetics and Mechanism of Solar-Thermochemical H2 Production by Oxidation of a Cobalt Ferrite-Zirconia Composite. *Energ. Environ. Sci.* 6 (3), 963–973. doi:10.1039/C3EE23568H

Scheffe, J. R., and Steinfeld, A. (2014). Oxygen Exchange Materials for Solar Thermochemical Splitting of H2O and CO2: A Review. *Mater. Today* 17 (7), 341–348. doi:10.1016/j.mattod.2014.04.025

Shannon, R. D. (1976). Revised Effective Ionic Radii and Systematic Studies of Interatomic Distances in Halides and Chalcogenides. *Acta Cryst. Sect A.* 32 (5), 751–767. doi:10.1107/S0567739476001551

Siegel, N. P., Miller, J. E., Ermanoski, I., Diver, R. B., and Stechel, E. B. (2013). Factors Affecting the Efficiency of Solar Driven Metal Oxide Thermochemical Cycles. *Ind. Eng. Chem. Res.* 52 (9), 3276–3286. doi:10.1021/ie400193q

Singstock, N. R., Bartel, C. J., Holder, A. M., and Musgrave, C. B. (2020). High-Throughput Analysis of Materials for Chemical Looping Processes. *Adv. Energ. Mater.* 10 (27), 2000685. doi:10.1002/aenm.202000685

Smestad, G. P., and Steinfeld, A. (2012). Review: Photochemical and Thermochemical Production of Solar Fuels from H2O and CO2 Using Metal Oxide Catalysts. *Ind. Eng. Chem. Res.* 51 (37), 11828–11840. doi:10.1021/ie3007962

Steinfeld, A. (2005). Solar Thermochemical Production of Hydrogen-Aa Review. *Solar Energy* 78 (5), 603–615. doi:10.1016/j.solener.2003.12.012

Tamaura, Y., Steinfeld, A., Kuhn, P., and Ehrensberger, K. (1995). Production of Solar Hydrogen by a Novel, 2-Step, Water-Splitting Thermochemical Cycle. *Energy* 20 (4), 325–330. doi:10.1016/0360-5442(94)00099-O

Toby, B. H., and Von Dreele, R. B. (2013). GSAS-II: The Genesis of a Modern Open-Source All Purpose Crystallography Software Package. *J. Appl. Cryst.* 46, 544–549. doi:10.1107/s0021889813003531

Vasala, S., and Karppinen, M. (2015). A2B′B″O6 Perovskites: A Review. *Prog. Solid State. Chem.* 43 (1), 1–36. doi:10.1016/j.progsolidstchem.2014.08.001

Wiglusz, R. J., Kordek, K., Małecka, M., Ciupa, A., Ptak, M., Pazik, R., et al. (2015). A New Approach in the Synthesis of La1−xGdxFeO3 Perovskite Nanoparticles - Structural and Magnetic Characterization. *Dalton Trans.* 44 (46), 20067–20074. doi:10.1039/C5DT03378K

Yang, C.-K., Yamazaki, Y., Aydin, A., and Haile, S. M. (2014). Thermodynamic and Kinetic Assessments of Strontium-Doped Lanthanum Manganite Perovskites for Two-step Thermochemical Water Splitting. *J. Mater. Chem. A.* 2 (33), 13612–13623. doi:10.1039/C4TA02694B

Conflict of Interest: The authors declare that the research was conducted in the absence of any commercial or financial relationships that could be construed as a potential conflict of interest.

Publisher's Note: All claims expressed in this article are solely those of the authors and do not necessarily represent those of their affiliated organizations, or those of the publisher, the editors and the reviewers. Any product that may be evaluated in this article, or claim that may be made by its manufacturer, is not guaranteed or endorsed by the publisher.